Journal Pre-proof

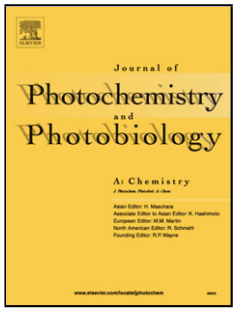

Synthesis and Preliminary Photopolymerization Evaluation of Novel Photoinitiators Containing Phototrigger to Overcome Oxygen Inhibition in the UV- Curing System

Wenbin Chen, Lei Wang, Xinyue Liu, Bo Chen, Guofeng Zhao

PII: S1010-6030(19)31421-2

DOI: https://doi.org/10.1016/j.jphotochem.2019.112187

Reference: JPC 112187

To appear in: *Journal of Photochemistry & Photobiology, A: Chemistry*

Received Date: 20 August 2019

Revised Date: 16 October 2019

Accepted Date: 21 October 2019

Please cite this article as: Chen W, Wang L, Liu X, Chen B, Zhao G, Synthesis and Preliminary Photopolymerization Evaluation of Novel Photoinitiators Containing Phototrigger to Overcome Oxygen Inhibition in the UV- Curing System, *Journal of Photochemistry and amp; Photobiology, A: Chemistry* (2019), doi: https://doi.org/10.1016/j.jphotochem.2019.112187

Synthesis and Preliminary Photopolymerization Evaluation of Novel Photoinitiators Containing Phototrigger to Overcome Oxygen Inhibition in the UV- Curing System

Wenbin Chen*, Lei Wang, Xinyue Liu, Bo Chen, Guofeng Zhao*

State Key Laboratory and Institute of Elemento-Organic Chemistry, College of Chemistry, Nankai University, Tianjin, 300071, China

Graphical abstract:

Two novel kinds of photoinitiators containing photo-trigger have good overcoming oxygen inhibition in the UV-curing system

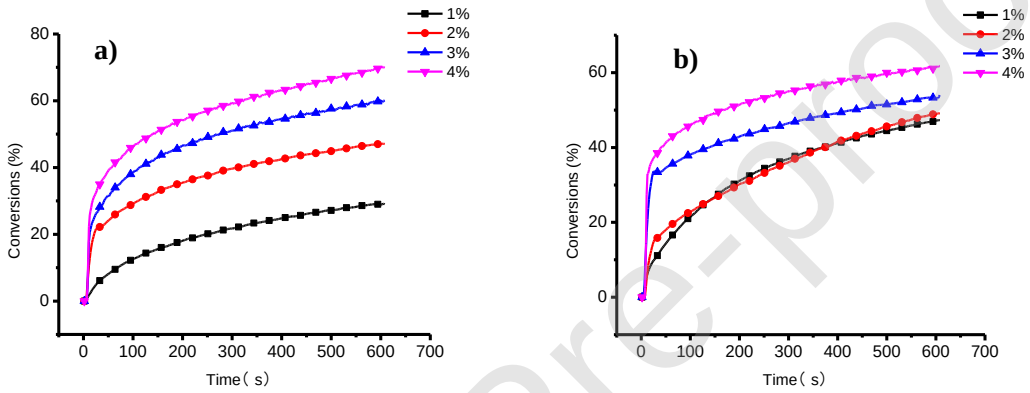

Highlight

- Two novel kinds of photoinitiators containing photo-trigger were synthesized
- The spectral properties show remarkable redshift compared to the references
- The photo-initiating activity of the initiators was evaluated by real-time FT-IR (RT-FTIR)
- The synthesized photoinitiators show good overcoming oxygen inhibition
- The synthesized photoinitiators can be used as one-component initiators

Abstract

In this work, two types of novel photoinitiaors containing phototrigger were prepared to overcome oxygen inhibition in the UV- curing system in the absence of hydrogen donor. The structures of prepared novel photoinitiators were determined by nuclear magnetic resonance (NMR) and high resolution MS (HR-MS) spectra data. The photo chemical behavior and photo-reactivity were also evaluated by ultraviolet-visible (UV-vis) spectroscopy and real-time Fourier transform infrared spectroscopy (RT-FTIR), respectively. The results show the prepared photoinitiators exhibit remarkable redshift compared to the commercial BP (benzophenone) and Irgacure 907 (2-methyl-1-(4-methylsulfanylphenyl)-2-morpholin- 4-ylpropan-1-one), fast photolysis by C-S

* Corresponding authors
E-mail addresses: wbchen@nankai.edu.cn (W. B. Chen) gfzhao@nankai.edu.cn (G. F. Zhao)

bond, good photo initiation and significant overcoming oxygen inhibition for some compounds, which can be used as one-component photoinitiator candidates.

Keywords: Photoinitiator, Photopolymerization, Phototrigger, Oxygen inhibition

1. Introduction

Photoinitiated polymerization is widely used in numerous fields such as coatings, adhesives, inks, dentistry, medicine, microelectronics and so on [1-3]. In recent years, UV-based 3D-printing, being one of the most revolutionary and powerful tools, has attracted the public interest because of the smart manufacturing on demand [1, 4, 5]. Photoinitiator is the most important component of coating formulation, which absorbs UV radiation and generates active radicals to initiate the polymerization [6]. There are two kinds of photoinitiators, radical photoinitiators and cationic photoinitiators. The former include Type I or α-cleavage and Type II photoinitiators. Type I photoinitiators undergo photo cleavage resulting in two radical species, both being capable of initiating the polymerization, while Type II initiators generate radicals in the presence of a co-initiator, typically hydrogen donating compounds, such as amines, thiols or alcohols[3]. The cationic photo-polymerization also receives considerable attention in industry and academia mainly due to its insensitivity to oxygen [7]. But because of the wide use of monomers and photoinitiators, greater effort has been dedicated to free radical photoinitiating systems than the effort to cationic photopolymerization.

Even though the UV-curing technique has great benefits of high efficiency, low energy consumption, and being solvent-free and environmentally friendly, the free radical polymerization has some shortcomings, such as odor, oxygen inhibition, yellowing, migration, and poor compatibility with the UV-curable resin, which will lead to undesirable effects in the post-cured materials. Because the UV-curing is operated in the air, the oxygen diffuses from the atmosphere into the formulation and reacts with excited species and radicals to quench the UV-curing, and results in diminished mechanical performance and tacky surface [8]. So the oxygen inhibition is another major obstacle and challenge besides migration and yellowing. There are many tactics to overcome oxygen inhibition of UV-curing procedure. These strategies include physical and chemical methods [9]. The former is the oldest and most widespread strategy, which prevents diffusion of oxygen from the atmosphere into the polymerizing resin by introducing inert gas (nitrogen, argon, carbon dioxide) or physical barriers. On the other hand, increasing curing light intensity and concentration of photoinitiator are known to be the easiest way to mitigate oxygen inhibition, but it will result in light shielding, volume shrinkage, and especially higher industrial cost [10].

In addition to the physical methods, a lot of chemical strategies have been developed over the years to overcome oxygen inhibition. Chemical strategies are divided into the adding of additive in the formulation and modification of the monomers, photoiniators or oligomers in the formulation. The effective additive materials that can consume the oxygen during curing process are tertiary amine [9], thiol [11] and triphenylphosphine (TPP) [12]. Thiol is usually used as additive in the curing formulation to reduce the effect of oxygen inhibition by undergoing chain transfer with the peroxide radical because of the high reactive thiol-ene click reaction. Beyond reducing the oxygen inhibition, the thiols functional curing materials also exhibit many other

properties such as low polymerization shrinkage [13], red shift of absorption maximum [14], great mechanical property [11] and photolysis reactions at the C–S bond as in a type I system [15].

Despite many potential desirable characteristics, there are a few drawbacks of thiols additive UV curable systems, most notably odor and bad stability. It is a big challenge to combine the advantages of overcoming oxygen inhibition and the disadvantages of odor and instability in the UV curing materials. It is a good strategy to protect the thiol with a protective group to eliminate the odor and instability, and then it will be released when exposed to light. Phototrigger is a good protective group to eliminate the odor and instability of thiol, which will be removed under photo initiation to release the thiol to overcome oxygen inhibition, and it has also been used widely in organic synthesis and biology [16].

Herein, we report two types of novel photoinitiators containing phototrigger to protect thiol and evaluate their photoreactivity and oxygen scavenging effect in photopolymerization process by real-time Fourier transform infrared spectroscopy (RT-FTIR). The phototrigger arylcarbonylmethyl group can undergo photoinitiated breaking of the C−S bond [17], which was used as a protective to prepare the novel photoinitiators. The detailed synthetic route is depicted in Scheme 1.

2. Experimental

2.1. Materials and instruments

All chemicals and solvents used for synthesis were purchased from commercial suppliers and used directly in the experiments without further purification. The progress of the reactions was monitored by thin layer chromatography (TLC) on pre-coated silica gel 60 F254 plates and spots were visualized by UV light. Flash-column chromatography was performed using commercial grades of silica gel 200-300 meshes. ^{1}H NMR and ^{13}C NMR spectra were recorded on a Bruker 400 spectrometer in $CDCl_3$. Chemical shifts are reported in parts per million relative to internal standard tetramethylsilane (TMS = 0.00 ppm). Coupling constants (*J*) are reported in Hertz (Hz). High-resolution mass spectra (HR-MS) were obtained on a Varian 7.0 T FTICR-MS. The UV-visible spectra were recorded on a L5 spectrophotometer (INESA, China). Photopolymerization kinetics studies were obtained on a Nicolet 5700 real-time infrared spectrometer (RT-FTIR), (Thermo Fisher, USA). Melting point was recorded on a WRS-2 melting point apparatus from Shanghai Shenguang Instruments Co., Ltd.

1, 6-hexanediol diacrylate (HDDA), 2-(2-ethoxyethoxy) ethyl acrylate (EOEOEA), trimethylolpropane triacrylate (TMPTA), tripropylene glycol diacrylate (TPGDA) were obtained from Tianjin Jiuri New Materials Co. Ltd.

The photosensitive formulations were deposited on a KBr pellet in laminate for irradiation with xenon lamp (XD 300, I = 28 mW cm^{-2}).

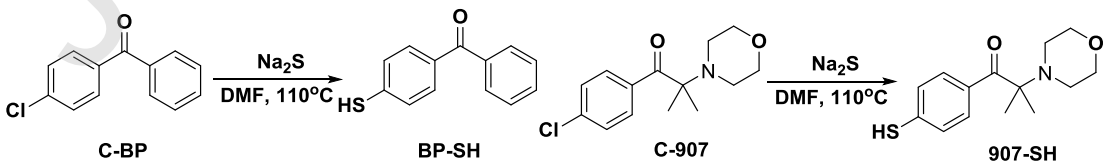

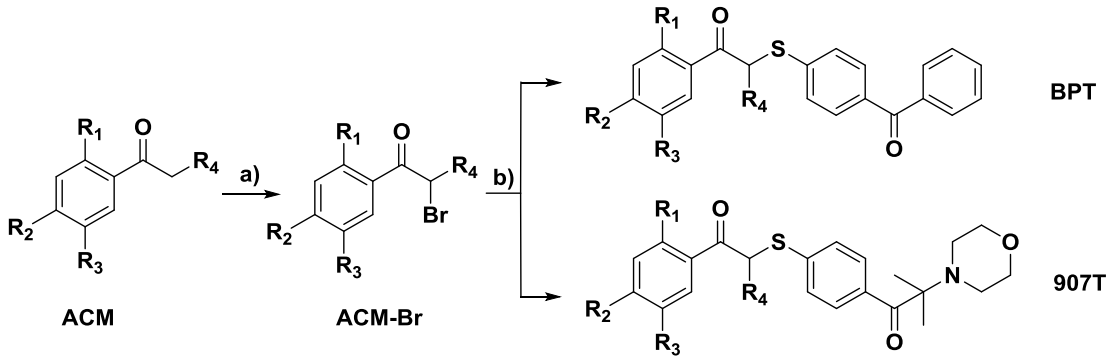

ACM-Br-a, BPT-a, 907T-a: R_1=H, R_2=H, R_3=H, R_4= H
ACM-Br-b, BPT-b, 907T-b: R_1=CH_3, R_2=H, R_3=H, R_4= H
ACM-Br-c, BPT-c, 907T-c: R_1=H, R_2=OH, R_3=H, R_4= H
ACM-Br-d, BPT-d, 907T-d: R_1=H, R_2=OH, R_3=H, R_4=CH_3
ACM-Br-e, BPT-e, 907T-e: R_1=H, R_2=OH, R_3=OCH_3, R_4=H
ACM-Br-f, BPT-f, 907T-f: R_1=H, R_2=OCH_3, R_3=OCH_3, R_4=H
ACM-Br-g, BPT-g, 907T-g: R_1=H, R_2-R_3=OCH_2O, R_4=H

Scheme 1 The synthetic routes to photoinitiators BPT and 907T

2.2 Preparation of BP-SH and 907-SH

2.2.1 4-Mercaptobenzophenone (BP-SH) [18]

To the mixture of 4-chlorobenzophenone (20.0 g, 92.3 mmol) in 200 mL of DMF was added $Na_2S·9H_2O$ (80.0 g, 333.1 mmol) with mechanical stirring. The mixture was heated to 110 °C for 12 h. The reactant was cooled to room temperature and poured into 200 mL of water, and adjusted to pH 5-6 with 15% HCl aqueous. The light yellow precipitate was filtered and dissolved in 100 mL of toluene, washed with 5% NaOH aqueous (50 mL × 3). The organic phase was acidified to pH 3-5 with 15% HCl aqueous, the precipitate was filtered and washed with water, dried to a white solid, m. p., 72-74°C, 9.2 g (42.9 mmol), 46.5%. ^{1}H NMR (400 MHz, $CDCl_3$) δ/ppm 7.76 (d, *J* = 7.3 Hz, 2H) , 7.69 (d, *J* = 8.3 Hz, 2H)， 7.58 (t, *J* = 7.4 Hz, 1H) , 7.48 (t, *J* = 7.6 Hz, 2H) , 7.33 (d, *J* = 8.3 Hz, 2H) , 3.65 (s, 1H) . ^{13}C NMR (101 MHz, $CDCl_3$) δ/pm 195.7, 138.1, 137.6, 134.4, 132.3, 130.9, 129.8, 128.3, 128.0

2.2.2 1-(4-Mercaptophenyl)-2-methyl-2-morpholinopropan-1-one (907-SH) [19]

In a 500 mL four-necked flask equipped with mechanical stirring, dropping funnel and thermometer, was filled with $Na_2S·9H_2O$ (22.0 g, 91.5 mmol), anhydrous Na_2SO_4 (13.5 g, 112 mmol), NMP (60.0 g). After the mixture was heated to 75 °C, 1-(4-chlorophenyl)-2-methyl-2-morpholinopropan-1-one (C-907) (10.0 g, 37.3 mmol) in 20 g of NMP was added to the above mixture. After addition, the mixture was heated to 130 °C for 2 h. The reactant was cooled to room temperature, Na_2SO_4 was filtered off, and washed with NMP. The filtrate was poured into 200 mL of ice-water, adjusted with 15% HCl to pH 6-7 and stirred at room temperature for 1 h, and extracted with ether (50 mL × 3). The ether phase was concentrated to 25 mL, and washed with 5%

NaOH (15 mL × 3). The aqueous phase was separated and acidified to pH 6-7 with 15% HCl, and extracted with CH_2Cl_2 (25 mL × 3), dried over Na_2SO_4, concentrated and the residue was separated by silica gel chromatography with hexane/ethyl acetate (V/V 12.5:1) as eluent to obtain a white solid, 4.4 g (16.6 mmol, 44%). ^{1}H NMR (400 MHz, $CDCl_3$) δ/ppm 8.45 (d, *J* = 8.4 Hz, 2H), 7.25 (s, 2H), 3.74 - 3.64 (m, 4H), 3.60 (s, 1H)，2.61- 2.53 (m, 4H), 1.30 (s, 6H); ^{13}C NMR (101 MHz, $CDCl_3$) δ/ppm 202.2, 137.9, 132.6, 131.1, 127.6, 68.4, 67.4, 47.0, 20.2

2.3 1-Bromo-arylcarbonyl methyl intermediate (ACM-Br) [20-22]

General procedure: (substituted) acetophenone or propiophenone (ACM) (1.0 eq) was dissolved in the mixture solvent of chloroform and ethyl acetate (1:1) and then heated to reflux, $CuBr_2$ (1.6-2.0eq) was added in portions. The reaction was monitored by HPLC (mobile phase: acetonitrile/H_2O = 40:60, 1 mL/min, 20min, 254nm). After reaction, the mixture was filtered and washed with solvent, the filtrate was evaporated, and the residue was purified by flash column chromatography on silica gel to give intermediates ACM-Br.

ACM-Br-a: 2-bromo-1-phenylethanone, white solid, yield 54.7 %.

^{1}H NMR (400 MHz, $CDCl_3$) δ/ppm 8.01 (d, *J* = 8.5 Hz, 2H), 7.64 (t, *J* = 7.4 Hz, 1H), 7.52 (t, *J* = 7.7 Hz, 2H), 4.49 (s, 2H). ^{13}C NMR (101 MHz, $CDCl_3$) δ/ppm 191.3, 134.0, 133.9, 128.95, 128.9, 30.9.

ACM-Br-b: 2-bromo-1-(o-tolyl) ethanone, light yellow oil, yield 51.4 %.

^{1}H NMR (400 MHz, $CDCl_3$) δ/ppm 7.66 (dd, *J* = 5.6, 2.9 Hz, 1H), 7.44-7.38 (m, 1H), 7.29-7.24 (m, 2H), 4.42 (s, 2H), 2.51 (s, 3H). ^{13}C NMR (101 MHz, $CDCl_3$) δ 194.2, 139.7, 134.4, 132.4, 132.3, 129.1, 125.8, 33.9, 21.5.

ACM-Br-c: 2-bromo-1-(4-hydroxyphenyl) ethanone, light yellow powder, yield 50.8 %. ^{1}H NMR (400 MHz, DMSO) δ/ppm 10.53 (s, 1H), 7.89 (d, *J* = 8.7 Hz, 2H), 6.87 (d, *J* = 8.7 Hz, 2H), 4.78 (s, 2H). ^{13}C NMR (101 MHz, DMSO) δ/ppm 189.8, 162.6, 131.4, 125.4, 115.4, 33.4.

ACM-Br-d: 2-bromo-1-(4-hydroxyphenyl) propan-1-one, white solid, yield 61.3 %. ^{1}H NMR (400 MHz, DMSO) δ/ppm 10.54 (s, 1H), 7.93 (d, *J* = 8.8 Hz, 2H), 6.88 (d, *J* = 8.9 Hz, 2H), 5.73 (q, *J* = 6.5 Hz, 1H), 1.74 (d, *J* = 6.5 Hz, 3H).^{13}C NMR (101 MHz, DMSO) δ 191.8, 162.0, 131.1, 124.9, 115.2, 42.9, 20.2.

ACM-Br-e: 2-bromo-1-(4-hydroxy-3-methoxyphenyl) ethanone, white solid, 50.9 %. ^{1}H NMR (400 MHz, DMSO) δ/ppm 10.18 (s, 1H), 7.57 (d, *J* = 8.3 Hz, 1H), 7.49 (s, 1H), 6.89 (d, *J* = 8.3 Hz, 1H), 4.81 (s, 2H), 3.84 (s, 3H).^{13}C NMR (101 MHz, DMSO) δ 189.9, 152.4, 147.7, 125.7, 124.0, 115.1, 111.91, 55.7, 33.4.

ACM-Br-f: 2-bromo-1-(3, 4-dimethoxyphenyl) ethanone, pale yellow solid, yield 41 %. ^{1}H NMR (400 MHz, DMSO) δ /ppm 7.71 (d, *J* = 8.5 Hz, 1H), 7.49 (s, 1H), 7.09 (d, *J* = 8.5 Hz, 1H), 4.88 (s, 2H), 3.87 (s, 3H), 3.84 (s, 3H).^{13}C NMR (101 MHz, DMSO) δ 190.2, 153.6, 148.7, 126.7, 123.8,

110.9, 110.8, 55.8, 55.6, 33.5.

ACM-Br-g: 1-(benzo[d][1,3]dioxol-5-yl)-2-bromoethanone, white solid, yield 53.9 %. ^{1}H NMR (400 MHz, $CDCl_3$) δ/ppm 7.58 (dd, *J* = 8.2, 1.8 Hz, 1H), 7.44 (d, *J* = 1.7 Hz, 1H), 6.87 (d, *J* = 8.2 Hz, 1H), 6.07 (s, 2H), 4.38 (s, 2H).^{13}C NMR (101 MHz, $CDCl_3$) δ 189.6, 152.6, 148.5, 128.6, 125.6, 108.5, 108.1, 102.2, 30.7.

2.4 Preparation of photoinitiator BPT and 907T [23-26]

General procedure: To a stirred and refluxed solution of thiol compound BP-SH or 907-SH (1.0 eq), K_2CO_3 (1.2 eq) in acetone (20 mL), was added dropwise bromo-arylcarbonyl methyl intermediate ACM-Br (1.0 eq) in acetone (10 mL). After completion of the addition, the reaction was allowed to reflux until there was no starting material monitored by TLC. Then the reactant was cooled to room temperature, filtered, and concentrated. The resulting residue was purified by flash column chromatography on silica gel or recrystallized to afford the desired product.

BPT-a, 2-((4-benzoylphenyl)thio)-1-phenylethanone, white metallic glossy solid, m.p.108.6 °C, yield, 65.8 %.

^{1}H NMR (400 MHz, $CDCl_3$) δ/ppm 8.00 (d, *J* = 7.4 Hz, 2H), 7.76 (d, *J* = 7.2 Hz, 2H), 7.73 (d, *J* = 8.4 Hz, 2H), 7.60 (dt, *J* = 14.5, 7.4 Hz, 2H), 7.53 - 7.47 (m, 4H), 7.42 (d, *J* = 8.4 Hz, 2H), 4.42 (s, 2H).

^{13}C NMR (101 MHz, $CDCl_3$) δ/ppm 195.7, 193.4, 141.6, 137.6, 135.2, 133.8, 132.4, 130.7, 129.9, 128.7, 128.3, 127.5, 99.9, 39.6

HR-MS (ESI, m/z) Calcd. for $C_{21}H_{16}O_2S$ 332.0871(M^+), found 332.0866(M^+)

BPT-b, 2-((4-benzoylphenyl)thio)-1-(o-tolyl)ethanone, light yellow powder, m.p. 96.5 °C, yield 56.7 %.

^{1}H NMR (400 MHz, $CDCl_3$) δ /ppm 7.79 (d, *J* = 7.4 Hz, 2H), 7.75 (d, *J* = 8.3 Hz, 2H), 7.70 (d, *J* = 7.7 Hz, 1H), 7.62 (t, *J* = 7.4 Hz, 1H), 7.51 (t, *J* = 7.6 Hz, 2H), 7.43 (t, *J* = 8.6 Hz, 3H), 7.32 (t, *J* = 7.7 Hz, 2H), 4.40 (s, 2H), 2.48 (s, 3H).

^{13}C NMR (101 MHz, $CDCl_3$) δ/ppm 196.9, 195.7, 141.7, 139.3, 137.6, 135.8, 135.0, 132.3, 132.2, 132.0, 130.7, 129.8, 128.7, 128.3, 127.3, 125.7, 41.9, 21.2.

HR-MS (ESI, m/z) Calcd. for $C_{22}H_{18}O_2S$ 346.1028(M^+), found 346.1021(M^+)

BPT-c, 2-((4-benzoylphenyl)thio)-1-(4-hydroxyphenyl)ethanone, light yellow solid, m.p. 138.2 °C, yield 66.7 %.

^{1}H NMR (400 MHz, DMSO) δ/ppm 10.51 (s, 1H), 7.97 (d, *J* = 8.6 Hz, 2H), 7.71 (d, *J* = 7.3 Hz, 2H), 7.69 – 7.64 (m, 3H), 7.56 (t, *J* = 7.5 Hz, 2H), 7.49 (d, *J* = 8.3 Hz, 2H), 6.90 (d, *J* = 8.6 Hz, 2H), 4.77 (s, 2H).

^{13}C NMR (101 MHz, DMSO) δ/ppm 194.78, 191.8, 162.5, 143.0, 137.2, 133.4, 132.4, 131.2, 130.1, 129.3, 128.5, 126.7, 126.2, 115.3, 38.6.

HR-MS (ESI, m/z) Calcd. for $C_{21}H_{16}O_3S$ 348.0820 (M^+), found 348.0814 (M^+)

BPT-d, 2-((4-benzoylphenyl)thio)-1-(4-hydroxyphenyl)propan-1-one, white solid, m.p. 119.3 °C, yield 60.2%

^{1}H NMR (400 MHz, DMSO) δ/ppm 10.52 (s, 1H), 7.95 (d, *J* = 8.8 Hz, 2H), 7.75 – 7.64 (m, 5H), 7.57 (t, *J* = 7.6 Hz, 2H), 7.53 (d, *J* = 8.4 Hz, 2H), 6.87 (d, *J* = 8.8 Hz, 2H), 5.34 (q, *J* = 6.8 Hz, 1H), 1.51 (d, *J* = 6.8 Hz, 3H).

^{13}C NMR (101 MHz, DMSO) δ/ppm 194.8(ds), 162.5, 140.2, 136.9, 134.7, 132.6, 131.3, 130.2, 129.4, 129.3, 128.5, 126.1, 115.3, 44.4, 17.7.

HR-MS (ESI, m/z) Calcd. for $C_{22}H_{18}O_3S$ 362.0977 (M^+), found 385.0872 ($[M+Na]^+$)

BPT-e, 2-((4-benzoylphenyl)thio)-1-(4-hydroxy-3-methoxyphenyl)ethanone, white solid, m.p.141.1 °C, yield 74.2 %.

^{1}H NMR (400 MHz, $CDCl_3$) δ/ppm 7.76 (d, *J* = 7.1 Hz, 2H), 7.73 (d, *J* = 8.4 Hz, 2H), 7.61 – 7.54 (m, 3H), 7.48 (t, *J* = 7.6 Hz, 2H), 7.42 (d, *J* = 8.4 Hz, 2H), 6.98 (d, *J* = 8.2 Hz, 1H), 6.20 (s, 1H), 4.37 (s, 2H), 3.95 (s, 3H).

^{13}C NMR (101 MHz, $CDCl_3$) δ/ppm 195.7, 191.9, 151.1, 146.8, 142.1, 137.6, 134.9, 132.3, 130.7, 129.9, 128.3, 128.1, 127.3, 124.1, 114.0, 110.4, 56.1, 39.1.

HR-MS (ESI, m/z) Calcd. for $C_{22}H_{18}O_4S$ 378.0926 (M^+) found 378.0918(M^+)

BPT-f, 2-((4-benzoylphenyl)thio)-1-(3,4-dimethoxyphenyl)ethanone, white solid, m.p.143.6 °C, yield 67.4 %

^{1}H NMR (400 MHz, $CDCl_3$) δ/ppm 7.76 (d, *J* = 7.4 Hz, 2H), 7.74 (d, *J* = 8.4 Hz, 2H), 7.62 (d, *J* = 8.4 Hz, 1H), 7.59 (t, *J* = 7.4 Hz, 1H), 7.55 (s, 1H), 7.48 (t, *J* = 7.6 Hz, 2H), 7.43 (d, *J* = 8.4 Hz, 2H), 6.92 (d, *J* = 8.4 Hz, 1H), 4.38 (s, 2H), 3.97 (s, 3H), 3.94 (s, 3H).

^{13}C NMR (101 MHz, $CDCl_3$) δ/ppm 195.8, 192.1, 153.9, 149.2, 141.9, 137.5, 134.9, 132.4, 130.7, 129.9, 128.3, 128.3, 127.2, 123.5, 110.6, 110.1, 56.2, 56.1, 39.1.

HR-MS (ESI, m/z) Calcd. for $C_{23}H_{20}O_4S$ 392.1082 (M^+), found 392.1077 (M^+)

BPT-g, 1-(benzo[d][1,3]dioxol-5-yl)-2-((4-benzoylphenyl)thio)ethanone, white solid, m.p.157.4 °C, yield 69.0 %

^{1}H NMR (400 MHz, $CDCl_3$) δ/ppm 7.78 (dd, *J* = 12.9, 7.8 Hz, 4H), 7.65 – 7.59 (m, 2H), 7.55 – 7.47 (m, 3H), 7.44 (d, *J* = 8.4 Hz, 2H), 6.91 (d, *J* = 8.2 Hz, 1H), 6.10 (s, 2H), 4.37 (s, 2H).

^{13}C NMR (101 MHz, $CDCl_3$) δ/ppm 195.8, 191.5, 152.5, 148.4, 141.8, 137.5, 135.0, 132.4, 130.7, 129.9, 128.3, 127.3, 125.2, 108.4, 108.1, 102.1, 39.4.

HR-MS (ESI, m/z) Calcd. for $C_{22}H_{16}O_4S$ 376.0769 (M^+), found 377.0843$[M+H]^+$, 399.0650 $[M+Na]^+$

907T-a, 2-methyl-2-morpholino-1-(4-((2-oxo-2-phenylethyl)thio)phenyl)propan-1-one, yellow oil, yield 75.3 %

^{1}H NMR (400 MHz, $CDCl_3$) δ/ppm 8.49 (d, *J* = 8.5 Hz, 2H), 7.99 (d, *J* = 8.5 Hz, 2H), 7.62 (t, *J* = 7.4 Hz, 1H), 7.50 (t, *J* = 7.7 Hz, 2H), 7.34 (d, *J* = 8.6 Hz, 2H), 4.41 (s, 2H), 3.68 (t, *J* = 4.0 Hz, 4H), 2.56 (t, *J* = 4.0 Hz, 4H), 1.30 (s, 6H).

^{13}C NMR (101 MHz, $CDCl_3$) δ/ppm 202.26, 193.4, 141.5, 135.2, 133.8, 133.1, 130.9, 128.8, 128.6, 126.7, 68.4, 67.3, 47.0, 39.4, 20.2.

HR-MS (ESI, m/z) Calcd. for $C_{22}H_{25}NO_3S$ 383.1555 (M^+), found 384.1631$[M+H]^+$

907T-b, 2-methyl-2-morpholino-1-(4-((2-oxo-2-(o-tolyl)ethyl)thio)phenyl)propan-1-one, light yellow solid, m.p. 106.0 °C, yield 88.3 %.

^{1}H NMR (400 MHz, $CDCl_3$) δ/ppm 8.48 (d, *J* = 8.6 Hz, 2H), 7.68 (d, *J* = 7.9 Hz, 1H), 7.42 (t, *J* = 7.6 Hz, 1H), 7.31 (d, *J* = 8.6 Hz, 2H), 7.28 (t, *J* = 7.6 Hz, 1H), 7.27(s, 1H), 4.36 (s, 2H), 3.69 (t, *J* = 4.0 Hz, 4H), 2.56 (t, *J* = 4.0 Hz, 4H), 2.43 (s, 3H), 1.30 (s, 6H).

^{13}C NMR (101 MHz, $CDCl_3$) δ/ppm 202.2, 197.0, 141.5, 139.4, 135.8, 133.1, 132.3, 132.1, 130.9, 128.7, 126.6, 125.7, 68.4, 67.4, 47.0, 41.8, 21.3, 20.2.

HR-MS (ESI, m/z) Calcd. for $C_{23}H_{27}NO_3S$ 397.1712 (M^+), found 398.1787($[M+H]^+$)

907T-c, 1-(4-((2-(4-hydroxyphenyl)-2-oxoethyl)thio)phenyl)-2-methyl-2-morpholinopropan-1-one, yellow solid, m.p. 200.4 °C, yield 70.0 %

^{1}H NMR (400 MHz, DMSO) δ/ppm 10.52 (s, 1H), 8.41 (d, *J* = 8.5 Hz, 2H), 7.96 (d, *J* = 8.7 Hz, 2H), 7.39 (d, *J* = 8.6 Hz, 2H), 6.88 (d, *J* = 8.7 Hz, 2H), 4.75 (s, 2H), 3.57 (m, 4H), 2.46 (m, 4H), 1.22 (s, 6H).

^{13}C NMR (101 MHz, DMSO) δ/ppm 202.07, 192.4, 163.0, 143.1, 132.2, 131.7, 130.8, 127.2, 126.0, 115.7, 68.2, 67.0, 47.1, 38.9, 20.3.

HR-MS (ESI, m/z) Calcd. for $C_{22}H_{25}NO_4S$ 399.1504 (M^+), found 400.1579($[M+H]^+$)

907T-d, 1-(4-((1-(4-hydroxyphenyl)-1-oxopropan-2-yl)thio)phenyl)-2-methyl-2-morpholino-propan-1-one, white solid, m.p.155.7-156.4 °C yield 64.5 %

^{1}H NMR (400 MHz, DMSO) δ/ppm 10.50 (s, 1H), 8.39 (d, *J* = 8.6 Hz, 2H), 7.93 (d, *J* = 8.8 Hz, 2H), 7.44 (d, *J* = 8.6 Hz, 2H), 6.85 (d, *J* = 8.8 Hz, 2H), 5.31 (q, *J* = 6.7 Hz, 1H), 3.57 (t, *J* = 4.0 Hz, 4H), 2.45 (t, *J* = 4.0 Hz, 4H), 1.49 (d, *J* = 6.8 Hz, 3H), 1.22 (s, 6H).

^{13}C NMR (101 MHz, DMSO) δ/ppm 201.8, 194.9, 162.4, 139.9, 133.0, 131.3, 130.3, 128.5, 126.1, 115.3, 67.7, 66.4, 46.6, 44.2, 19.8, 17.8.

HR-MS (ESI, m/z) Calcd. for $C_{23}H_{27}NO_4S$ 413.1661 (M^+), found 414.1733 $[M+H]^+$, 436.1557 $[M+Na]^+$

907T-e, 1-(4-((2-(4-hydroxy-3-methoxyphenyl)-2-oxoethyl)thio)phenyl)-2-methyl-2- morpholino-propan-1-one, light yellow solid, m.p. 157.8 °C yield 55.7 %

^{1}H NMR (400 MHz, DMSO) δ/ppm 10.16 (s, 1H), 8.40 (d, *J* = 8.6 Hz, 2H), 7.65 (d, *J* = 8.3 Hz, 1H), 7.53 (s, 1H), 7.40 (d, *J* = 8.6 Hz, 2H), 6.90 (d, *J* = 8.3 Hz, 1H), 4.76 (s, 2H), 3.84 (s, 3H),

3.58 (t, *J* = 4.0 Hz, 4H), 2.45 (t, *J* = 4.0 Hz, 4H), 1.22 (s, 6H).

^{13}C NMR (101 MHz, DMSO) δ/ppm 201.5, 192.0, 152.2, 147.5, 142.6, 131.8, 130.3, 127.0, 125.6, 123.8, 114.9, 111.7, 67.7, 66.5, 55.6, 46.6, 38.4, 19.8.

HR-MS (ESI, m/z) Calcd. for $C_{23}H_{27}NO_5S$ 429.1610 (M^+), found 430.2000 ($[M+H]^+$)

907T-f, 1-(4-((2-(3, 4-dimethoxyphenyl)-2- oxoethyl)thio)phenyl)-2-methyl-2-morpholino-propan-1-one, orange solid, m.p.105.5 °C, yield 91.8 %

^{1}H NMR (400 MHz, $CDCl_3$) δ/ppm 8.49 (d, *J* = 8.5 Hz, 2H), 7.63 (d, *J* = 8.4Hz, 1H), 7.54 (s, 1H), 7.35 (d, *J* = 8.6 Hz, 2H), 6.91 (d, *J* = 8.4 Hz, 1H), 4.38 (s, 2H), 3.96 (s, 3H), 3.93 (s, 3H), 3.69 (t, *J* = 4.0 Hz, 4H), 2.56 (t, *J* = 4.0 Hz, 4H), 1.30 (s, 6H).

^{13}C NMR (101 MHz, $CDCl_3$) δ/ppm 202.2, 192.1, 153.8, 149.2, 141.8, 132.9, 130.9, 128.2, 126.5, 123.5, 110.6, 110.1, 68.4, 67.3, 56.1, 56.0, 47.0, 38.9, 20.1.

HR-MS (ESI, m/z) Calcd. for $C_{24}H_{29}NO_5S$ 443.1766 (M^+), found 444.1842 ($[M+H]^+$)

907T-g,1-(4-((2-(benzo[d][1,3]dioxol-5-yl)-2-oxoethyl)thio)phenyl)-2-methyl-2-morpholino-propan-1-one, white solid, m.p.138.2 °C yield 60.9 %

^{1}H NMR (400 MHz, $CDCl_3$) δ/ppm 8.49 (d, *J* = 8.5 Hz, 2H), 7.60 (dd, *J* = 8.2, 1.6 Hz, 1H), 7.46 (d, *J* = 1.3 Hz, 1H), 7.33 (d, *J* = 8.5 Hz, 2H), 6.88 (d, *J* = 8.2 Hz, 1H), 6.07 (s, 2H), 4.34 (s, 2H), 3.69 (t, *J* = 4.0 Hz, 4H), 2.56 (t, *J* = 4.0 Hz, 4H), 1.29 (d, *J* = 8.3 Hz, 6H).

^{13}C NMR (101 MHz, $CDCl_3$) δ/ppm 202.2, 191.6, 152.4, 148.4, 141.6, 133.1, 130.9, 129.9, 126.6, 125.2, 108.3, 108.1, 102.1, 68.4, 67.4, 47.0, 39.2, 20.2.

HR-MS (ESI, m/z) Calcd. for $C_{23}H_{25}NO_3S$ 427.1453 (M^+), found 428.1528 ($[M+H]^+$)

2.5 UV–vis spectral characterization of photoinitiators

The synthesized photoinitiators were dissolved in acetonitrile to prepare 1×10^{-4} mol/L stocking solution. The stocking solution was diluted to 8×10^{-5} mol/L, 6×10^{-5} mol/L, 4×10^{-5}mol/L, 2×10^{-5} mol/L samples, respectively. The UV-vis absorption spectra of the above samples were recorded on the L5 spectrophotometer using acetonitrile as blank. According to the Lambert-Beer law, equation (1), the standard curve was made and the molar absorption coefficient was calculated from the curve.

$$A=\varepsilon bc \qquad (1)$$

where C is the molar concentration of initiator, A is the absorption, ε is the molar absorption coefficient of initiator in acetonitrile (M^{-1} cm^{-1}), and b is the optical path length, (here 1 cm).

2.6 UV-Visible light photolysis experiment

The synthesized photoinitiators were dissolved in acetonitrile to prepare 2×10^{-5} mol/L solution. The solution was charged in a quartz cell and oxygen was removed by argon. The cell was sealed and exposed under a medium pressure mercury arc lamp (80mW/cm with output light intensity of 30mW/cm^2-40 mW/cm^2, measured with a UV radiometer capable of broad UV range coverage) for different time intervals at 0s, 2s, 5s, 10s, 20s, 30s, 40s, 50s. The photolysis fragments in solution were recorded on a HRESI-MS.

2.7 Photopolymerization kinetic experiments

The photopolymerization reactions of the multifunctional monomers (i.e., EOEOEA, HDDA TPGDA, TMPTA) in the presence of synthesized photoinitiator upon exposure to the UV point source OmniCure SERIES 1000 were monitored using the Nicolet 5700 real-time infrared (RT-FTIR) spectrometer. The prepared photocurable formulation was transferred on an infrared KBr salt plate to give a film thickness of 10 μm, and another KBr salt plate was used to cover the above KBr plate for preventing oxygen inhibition, while the evaluation of the overcoming oxygen inhibition for the synthesized photoinitiators were used only one KBr salt plate. The polymerization experiments were carried out by using a Nicolet 5700 RT-FTIR spectrometer to monitor the conversion percent of double bonds at intervals. The conversion of double bond (DC %) was calculated according to the equation (2) by measuring the peak area of 790-830 cm^{-1}.

$$DC(\%) = \frac{(A_0 - A_t)}{A_0} \times 100 \quad \ldots\ldots\ldots\ldots\ldots (2)$$

Where: A_0 represents the initial peak area before illumination, and A_t represents the area of the double bond absorption peak at time t.

Rates of polymerization were calculated according to the following formula (3) [27]:

$$Rp = \frac{d(DC)}{dt} \quad \ldots\ldots\ldots\ldots\ldots (3)$$

3. Results and discussion

3.1. Synthesis and characterization

The synthetic pathways to generate photoinitiator BPT and 907T are depicted in Scheme 1. The thiolated BP-SH and 907-SH are the key intermediates for the desired product. There are many methods to generate BPT-SH and 907-SH, sodium sulfide used as thiolated reagent is undoubtedly the best method from chlorinated C-BP and C-907, respectively. The appearance of the signal at 3.6 ppm was considered to be evidence of the introduction of mercapto group. 1-Bromo-arylcarbonyl methyl intermediate (ACM-Br) was obtained by $CuBr_2$ in refluxed mixture of chloroform and ethyl acetate, and monitored by HPLC in 40-60% yield, while NBS and Br_2 are active brominated reagents to give a complex.

As can be seen from ^{13}CNMR results, the presence of carbonyl peaks in the range of 190-195 ppm for BPT and 192-200 ppm for 907T in two singlets, respectively, indicates successful attachment of the BP-S and 907-S moiety. In addition, the high resolution MS data are in good agreement with the proposed structures.

3.2 Spectroscopic properties of photoinitiators

UV-vis absorption spectra of the prepared photoinitiators BPT and 907T were measured in acetonitrile with BP and 907 as the references. The corresponding values for the maximum absorption wavelength (λ_{max}) and the molar absorption coefficients (ε_{max}) at λ_{max} in CH_3CN are summarized in Table 1. The typical UV absorption spectra of BP, C-BP, BP-SH, BPT-b and 907, C-907, 907-SH, 907T-b are shown in Figure 1. From Figure 1 and Table 1, the maximum absorption of C-BP and C-907 are about 250-260 nm, while the mercapto BP-SH and 907-SH

exhibit significantly red-shifted absorption to about 290 nm. This result can be addressed to the strong electron-donating ability of the thiophenyl group and the key important n-π*-type transitions [28]. Similarly, the prepared photoinitiators BPT and 907T exhibit similar absorption characteristics as C-BP and C-907 or BP-SH and 907-SH but with a markedly red shift in solvent. The wavelengths for maximum absorption (λ_{max}) are above 300 nm due to increased electron donation via the sulfur atom and transannular conjugate effect via the benzoyl group. This would certainly account for the increased photoinitiation activity during photocuring [15].

Table 1 UV absorption properties of synthesized photoinitiators in acetonitrile

Photoinitiator	λ_{max} (nm)	ε_{max} (L/mol·cm)	Photoinitiator	λ_{max} (nm)	ε_{max} (L/mol·cm)
BP	251	1.520×10^4	907	304	6.063×10^4
C-BP	257	2.1240×10^4	C-907	251	1.2810×10^4
BP-SH	294	1.5390×10^4	907-SH	285	1.0810×10^4
BPT-a	308	1.0895×10^4	907T-a	300	1.4095×10^4
BPT-b	308	1.1561×10^4	907T-b	300	1.2415×10^4
BPT-c	287	1.0085×10^4	907T-c	288	1.0140×10^4
BPT-d	283	0.9240×10^4	907T-d	283	1.8160×10^4
BPT-e	307	0.9535×10^4	907T-e	305	0.7595×10^4
BPT-f	310	1.0140×10^4	907T-f	302	1.0170×10^4
BPT-g	311	1.0745×10^4	907T-g	306	0.5035×10^4

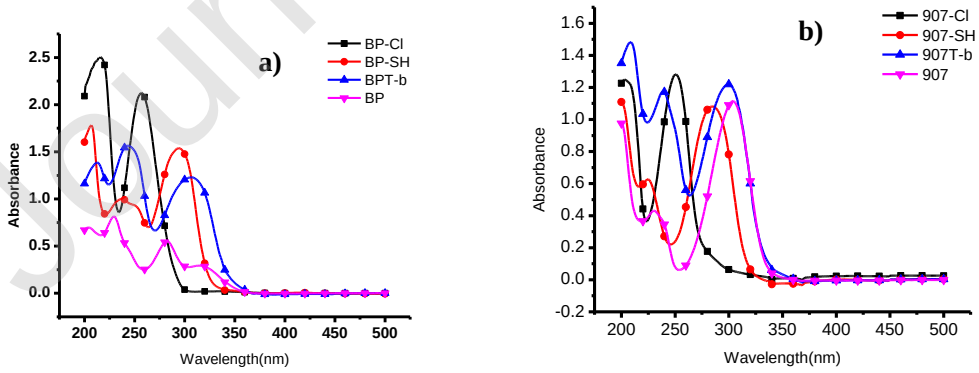

Fig. 1 UV-vis absorption spectra of some BP and 907 derivatives in CH_3CN (1×10^{-4} mol/L), **a)**: BP derivatives; **b)**: 907 derivatives

Photochemical change of the photoinitiator upon irradiation is an important issue for their use in photopolymerization processes. BPT and 907T were expected to undergo photolysis in the absence of hydrogen donors because of the hydrogen-donating thiol group in the structures. For this purpose, BPT-b and 907T-b were selected to study the UV-vis spectral changes of the initiators on irradiation in the absence of co-initiator and is shown in Fig. 2. The rapidly decreased absorbance maxima with time indicate the efficient photoreactivity of of BPT-b and 907T-b, which show that BPT-b and 907T-b are sensitive to irradiatation and have potential to be used as one component photoinitiator.

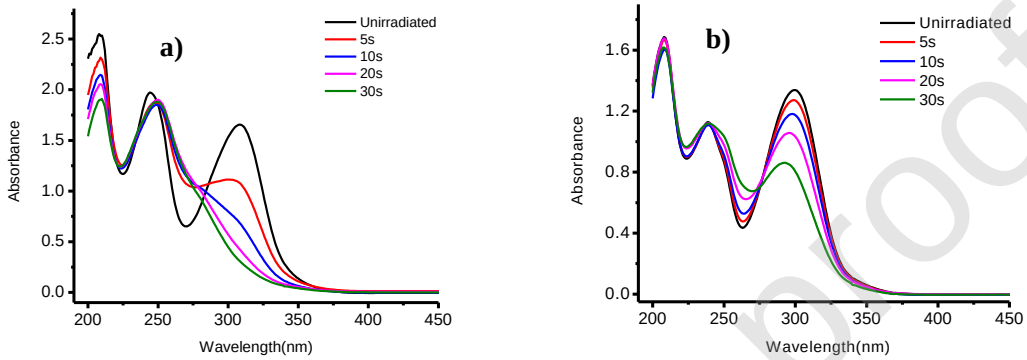

Fig. 2 UV-vis absorption spectral changes of BPT-b and 907T-b (2×10^{-5} mol/L) on irradiation under nitrogen in CH_3CN, **a)**: BPT-b; **b)**: 907T-b

To study the photolysis mechanism of the novel photoinitiators, we used HPLC and HR-MS to analyze the photolysis product after irradiation. As can be seen from Fig.3 and Table 2, the content of BPT-b and 907T-b in CH_3CN were decreased immediately after irradiation and the photolysis rate of BPT-b was faster than that of 907T-b. BPT-b was photolyzed almost completely within 20 seconds and 907T-b was photolyzed about 90% within 30 seconds. They were all photolyzed by breaking of the C-S bond after irradiation to form the thiol radical which was combined to generate the disulfide compound, which was confirmed by HR-MS with a molecular ion peak at 427.0820 $(M+H)^+$ for BPT-b and 529.2179 $(M+H)^+$ for 907T-b (Fig. 4 and Scheme 2).

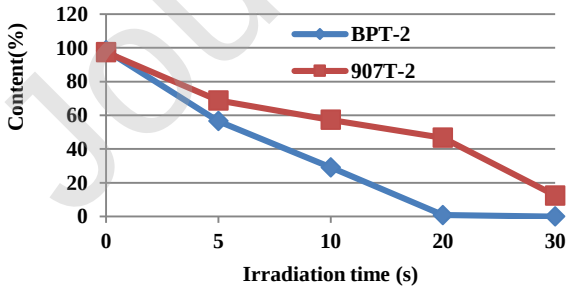

Fig. 3 The contents of initiators in CH_3CN under irradiation for different time

Table 2 The content of initiators in CH_3CN under irradiated for different time

Time	**BPT-2** (%)	**907T-2** (%)
5s	56.5075	68.8053
10s	29.1246	57.3383
20s	0.8112	46.6549
30s	0	12.4582

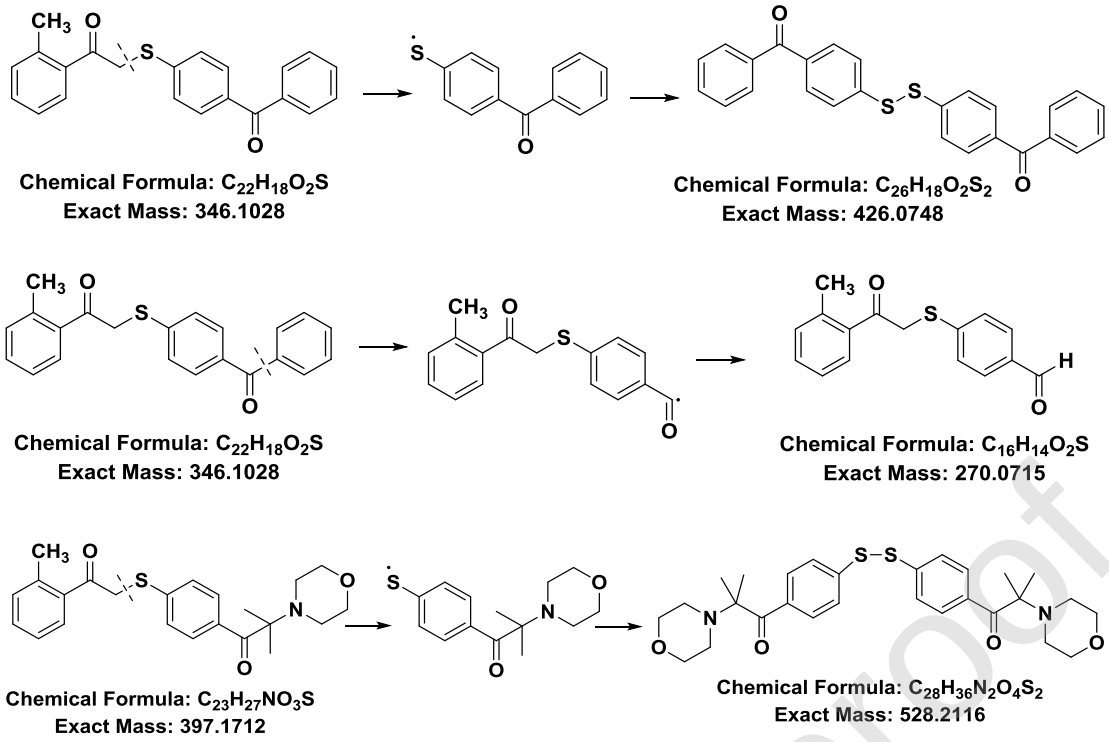

Scheme 2 Photolysis products of the BPT-b and 907T-b after irradiation

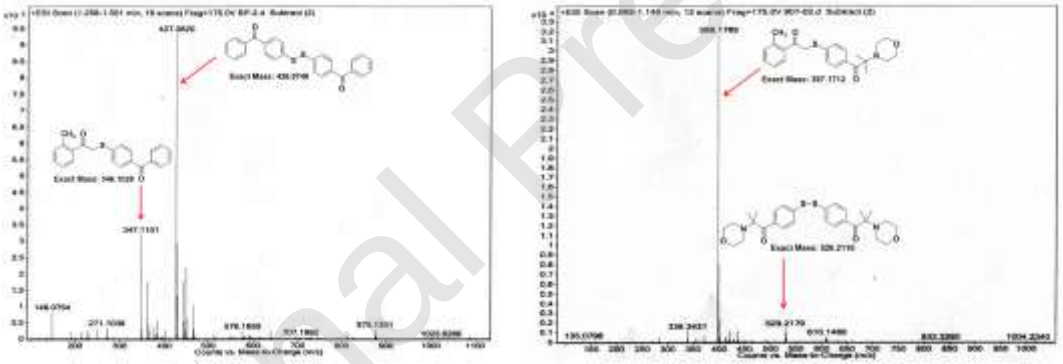

Fig. 4 HR-MS results for photolysis products of BPT-b and 907T-b

3.3 Photopolymerization activity study

To evaluate the photopolymerization efficiency of novel photoinitiators on acrylate curing, TPGDA was used as monomer, and mixed with photoinitiator content of 1.0 wt % using real-time FT-IR (RT-FTIR) in the absence of an additional hydrogen donor. Because BP could not initiate polymerization of TPGDA in the absence of hydrogen donor, the thiol photoinitiator BP-SH and 907-SH were used as references. The conversion-time and rate-time plots for the polymerization of samples cured under oxygen-free conditions are presented in Figure 5 and Figure 6.

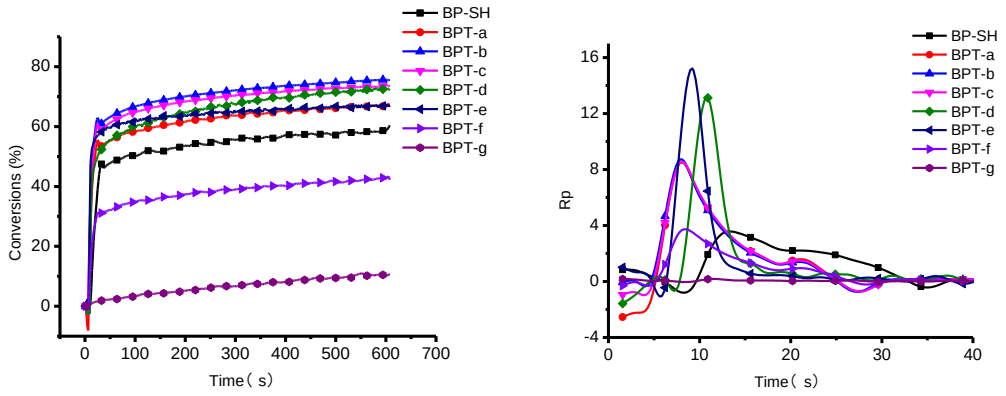

Fig. 5 Conversion-time and conversion rate (Rp) - time for the photopolymerization of TPGDA and different BPT initiators 1.0 wt % relative to monomer, light intensity 30 mW/cm^2

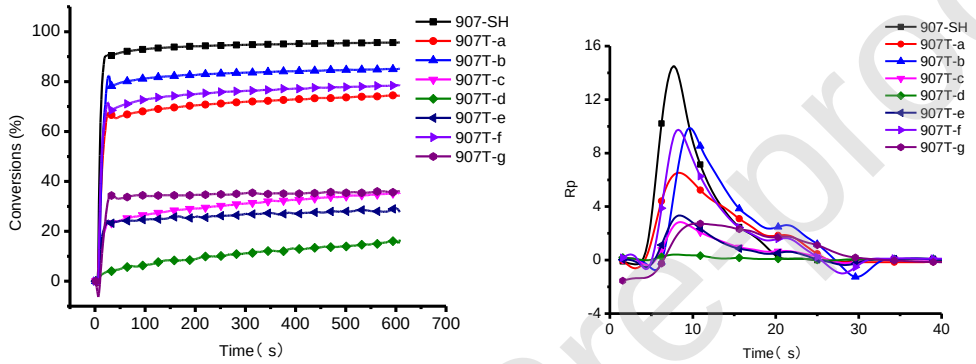

Fig.6 Conversion-time and conversion rate (Rp) - time for the photopolymerization of TPGDA and different 907T initiators 1.0 wt % relative to monomer, light intensity 30 mW/cm^2

As illustrated in Fig. 5 and Fig. 6, some BPT and 907T initiators are found to efficiently initiate photopolymerization under oxygen-free conditions and in the absence of an additional hydrogen donor. Although both types of initiators are effective in initiating the polymerization, 907T seems to be more photoactive in the curing process. The conversion of double bonds reaches its maximum within 10 s with a rapid first stage, but followed by a slow stage. This trend is also reflected in the RT-FTIR data from the Rp value. These results can be attributed to following reasons. First, the red-shifted maximum absorption would certainly account for its higher photoefficiency. Second, more radicals may be generated from the photolysis reaction of the C-S bond. Lastly, more radicals yielded could cause the monomers to polymerize rapidly [29]. Subsequently, the conversion did not increase due to the decrease in the concentration of photoinitiator, rapid increase of viscosity and a significant reduction in the mobility of large molecules because of gel effect and cage effect.

The conversion of TPGDA polymerization initiated by 907T-a, 907T-b and 907T-f are higher than 70%, but they are lower than that of 907-SH in the absence of oxygen. Notably, the conversion and rate of TPGDA polymerization initiated by BPT-a, BPT-b, BPT-c, BPT-d and BPT-e are higher than those initiated by BP-SH. It is presumed that BP series are type II photoinitiators and need co-initiators, and BP-SH needs one molecule as an initiator and one molecule as a co-initiator to provide active hydrogen to form active radicals to initiate polymerization, while other BP initiators can directly generate thiol radical to initiate

polymerization, and do not need the co-initiator.

We selected some photoinitiators with good photopolymerization activity under oxygen-free conditions to evaluate the oxygen scavenging effect. As can be seen from Fig. 7, BPT-a, BPT-b, BPT-c, BPT-d, BPT-e possess moderate oxygen scavenging activity, while 907T-b and 907T-f have good ability to overcome oxygen inhibition. Usually, under air condition, the rate of polymerization of TPGDA is very low and the final conversion hardly reaches 30% [12], however, 907T-b can reach about 50%. This result can be attributed to the photolysis reaction of the C-S bond to afford thiol radical to consume some oxygen, which reduced the oxygen inhibition. If the concentration of the photoinitiators increased, the overcoming oxygen inhibition of BPT-b and 907T-b show up more significantly. According to Fig. 8, when the concentrations of photoinitiators are gradually increased from 1.0% to 4.0wt% relative to monomer, the conversions of double bond vary from 40-60% for 907T-b and 30-70% for BPT-b under air, respectively.

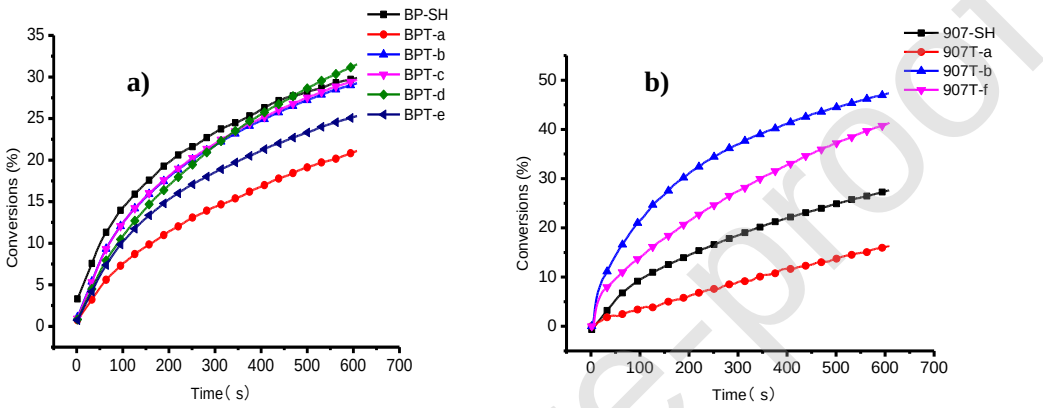

Fig. 7 Conversion-time for the photopolymerization of TPGDA for different initiators at 1.0 wt% under air, light intensity 30 mW/cm^2, **a)**: BP-SH and BPT derivatives; **b)**: 907-SH and 907T derivative

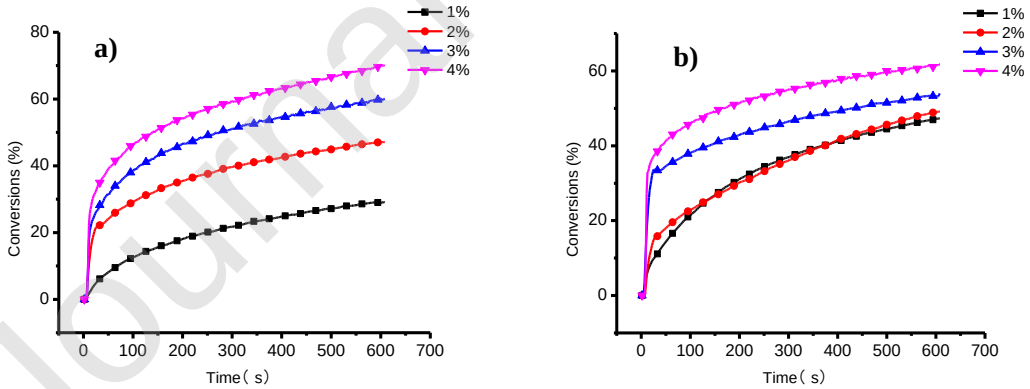

Fig. 8 Conversion-time for the photopolymerization of TPGDA at different concentrations of initiators under air, light intensity 30 mW/cm^2, **a**): BPT-b; **b**): 907T-b

Under oxygen-free condition, the concentration dependence was more significant, and Fig. 9 shows the conversion variation with the increasing content of prepared initiators. It can be seen that when the concentration of BPT-b is gradually increased from 1.0% to 4.0 wt% relative to monomer, the final double bond conversion is increased. However, the concentration of initiator

had little effect on the final conversion rate for 907T-b and the final conversion rate reached a higher percentage at 1.0 wt%.

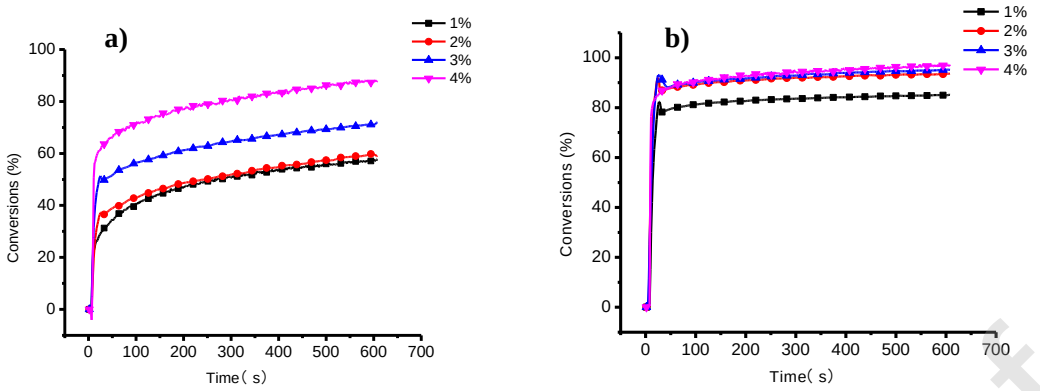

Fig. 9 Photopolymerization efficiency of different concentration of BPT-b and 907T-b for TPGDA under oxygen-free conditions, light intensity 30 mW/cm^2, **a**): BPT-b; **b**): 907T-b

Fig. 10 shows the conversion variation with the light intensity increasing. According to the Fig. 10, the maximum conversion rate rises from 50% to 80% with increased light intensity from 30 mW/cm^2 to 60 mW/cm^2 for BPT-b. It is easy to explain in that the higher light intensity can form more free radicals to induce the photopolymerization. However, the light intensity has little effect on the maximum conversion rate for 907T-b. This may be that 907T-b can generate more radicals at lower light intensity and it will be a good initiator candidate with good photo-activity and good ability to overcome oxygen inhibition, which can be used as type I and type II initiators.

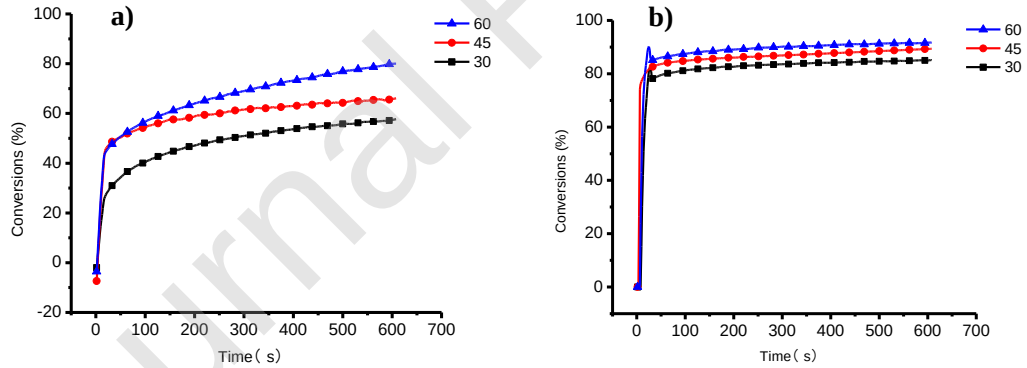

Fig. 10 Photopolymerization of TPGDA in different light intensity under oxygen free, BPT-b or 907T-b 1.0 wt%, **a)**: BPT-b; **b)**: 907T-b

Monomers not only play a role in dissolving and diluting oligomers and adjusting the viscosity of the curing system, but also participate in the curing process. They also influence the curing rate and the properties of the curing film. We evaluated the photopolymerization of different monomers with the synthesized initiator BPT-b or 907T-b. As can be seen from Fig.11, it is clear that the final double bond conversion of TPGDA initiated by 907T-b is much higher than HDDA and TMPTA, and same as EOEOEA. Moreover, the final double bond conversion of TPGDA and EOEOEA initiated by BPT-b is much higher than HDDA and TMPTA. Although TPGDA and HDDA have the same functionality, TPGDA has better flexibility and the polymerization rate is

faster than HDDA. TMPTA is a trifunctional monomer, and its final conversion rate is significantly lower than that of the difunctional methacrylate monomer because the chain growth reaction of the polymer is controlled by diffusion which is decreasing with the rapid increase of viscosity because of the gel effect [30-33].

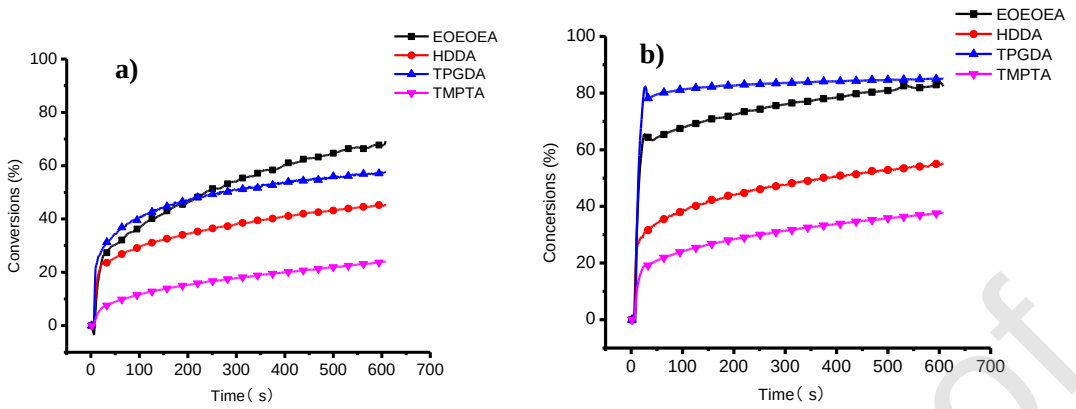

Fig. 11 Comparison of photopolymerization of monomer EOEOEA, TMPTA, HDDA and TPGDA under oxygen free, BPT-b or BPT-b 1.0 wt%, light intensity 30 mW/cm^2, **a)**: BPT-b; **b**): 907T-b

4. Conclusion

Here, two types of novel photoinitiators containing phototrigger were reported. The maximum absorption wavelength of the prepared initiators are more than 300 nm with remarkable redshift compared to BP (benzophenone) and Irgacure 907 (2-methyl-1-(4-methylsulfanylphenyl)-2-morpholin-4-ylpropan-1-one). The UV curing behavior analysis indicated that the double conversion rates were up to 50% under air conditions when the light intensity was 30 mW/cm^2, which is higher than for traditional photoinitiators. When the concentrations of photoinitiators are increased to 4.0wt%, the ability to overcome oxygen inhibition can be further improved by the conversion of double bond to about 60-70% in the absence of hydrogen donor, so the prepared initiators can be used as one-component initiator candidates.

Conflict of interest

The authors declared that they have no conflicts of interest to this work.

Acknowledgements

The authors thank Prof. Jun Nie and Prof. Xiaoqun Zhu from Beijing University of Chemical Technology for the support of the real-time infrared (RT-FTIR) spectrometer for free and the fruitful discussions with the group members on initiating systems. The authors are very grateful for financial support from Tianjin Jiuri New Materials Company Limited (No. 2018120024001216, No. 2017120024000913 and No. 2016120024001223).

References:

[1] B. Cesur, O. Karahan, S. Agopcan, T.N. Eren, N. Okte, D. Avci, Difunctional monomeric and polymeric photoinitiators: Synthesis and photoinitiating behaviors, Prog. Org. Coat., 86 (2015) 71-78.

[2] Y. Yagci, S. Jockusch, N.J. Turro, Photoinitiated Polymerization: Advances, Challenges, and Opportunities, Macromolecules, 43 (2010) 6245-6260.

[3] J. Kreutzer, K. Kaya, Y. Yagci, Poly(propylene oxide)-thioxanthone as one-component Type II polymeric photoinitiator for free radical polymerization with low migration behavior, Eur. Polym. J., 95 (2017) 71-81.

[4] W. Jamroz, J. Szafraniec, M. Kurek, R. Jachowicz, 3D Printing in pharmaceutical and medical applications - recent achievements and challenges, Pharm. Res., 35 (2018) 176.

[5] G.W. Ma, L. Wang, A critical review of preparation design and workability measurement of concrete material for largescale 3D printing, Front. Struct. Civ. Eng., 12 (2018) 382-400.

[6] E.A. Kandirmaz, N.K. Apohan, E.N. Gencoglu, Preparation of novel thioxanthone based polymeric photoinitiator for flexographic varnish and determination of their migration behaviour, Prog. Org. Coat., 119 (2018) 36-43.

[7] O.S. Taskin, I. Erel-Goktepe, M.A.A. Khan, S. Pispas, Y. Yagci, Polystyrene-b-poly(2-vinyl phenacyl pyridinium) salts as photoinitiators for free radical and cationic polymerizations and their photoinduced molecular associations, J. Photochem. Photobiol., A, 285 (2014) 30-36.

[8] J.Y. Zhou, X. Allonas, X.X. Liu, Fluorinated organozirconiums: Enhancement of overcoming oxygen inhibition in the UV-curing film, Prog. Org. Coat., 120 (2018) 228-233.

[9] S.C. Ligon, B. Husar, H. Wutzel, R. Holman, R. Liska, Strategies to reduce oxygen inhibition in photoinduced polymerization, Chem. Rev., 114 (2014) 557-589.

[10] S. Liang, Y.D. Yang, H.Y. Zhou, Y.Q. Li, J.X. Wang, Fluorinated photoinitiators: Synthesis and photochemical behaviors, Prog. Org. Coat., 114 (2018) 102-108.

[11] J.B. Wu, G.Z. Ma, P. Li, L.X. Ling, B.J. Wang, Preparation of multifunctional thiol- and acrylate-terminated polyurethane: A comparative study on their properties in UV curable coatings, J. Appl. Polym. Sci., 131 (2014) 40740.

[12] C. Belon, X. Allonas, C. Croutxe-Barghorn, J. Lalevee, Overcoming the oxygen inhibition in the photopolymerization of acrylates: A study of the beneficial effect of triphenylphosphine, J. Polym. Sci., Part A: Polym. Chem., 48 (2010) 2462-2469.

[13] N.B. Cramer, S.K. Reddy, M. Cole, C. Hoyle, C.N. Bowman, Initiation and kinetics of thiol-ene photopolymerizations without photoinitiators, J. Polym. Sci., Part A: Polym. Chem., 42 (2004) 5817-5826.

[14] N.S. Allen, M. Edge, F. Catalina, T. Corraies, M. Blanco-Pina, A. Green, Photochemistry and photocuring activities of novel substituted 4′-(4-methylphenylthio) benzophenones as photoinitiators, J. Photochem. Photobiol., A, 110 (1997) 183-190.

[15] N.S. Allen, T. Corrales, M. Edge, F. Catalina, C. Peinado, M. Blanco-Pinar, A. Green, Photochemistry and photopolymerisation activities of novel alkylthiobenzophenone photoinitiators, Eur. Polym. J., 34 (1998) 303-308.

[16] P. Klan, T. Solomek, C.G. Bochet, A. Blanc, R. Givens, M. Rubina, V. Popik, A. Kostikov, J. Wirz, Photoremovable Protecting Groups in Chemistry and Biology: Reaction Mechanisms and Efficacy, Chem. Rev., 113 (2013) 119-191.

[17] A.T. Veetil, T. Solomek, B.P. Ngoy, N. Pavlikova, D. Heger, P. Klan, Photochemistry of

S-phenacyl xanthates, J. Org. Chem., 76 (2011) 8232-8242.

[18] W.C. Zhao, Z.L. Ma, J. Li, L. Yao, J. zhang, W. Hu, Y. Wang, Mercapto benzophenone compounds, compositions and preparation method thereof, Insight High Technology (Beijing) Co Ltd, China, 2013.

[19] K. Fabian, G. Kai-Uwe, Y. Sakurai, T. Okuda, Michael addition reaction product and active energy ray-curable composition, DIC Corporation, Tokyo, Japan, 2012.

[20] M. Koura, T. Matsuda, A. Okuda, Y. Watanabe, Y. Yamaguchi, S. Kurobuchi, Y. Matsumoto, K. Shibuya, Design, synthesis and pharmacology of 1, 1-bistrifluoromethylcarbinol derivatives as liver X receptor β-selective agonists, Bioorg. Med. Chem. Lett., 25 (2015) 2668-2674.

[21] G. Blum, A. Gazit, A. Levitzki, Development of new insulin-like growth factor-1 receptor kinase inhibitors using catechol mimics, J. Biol. Chem., 278 (2003) 40442-40454.

[22] R. Aeluri, M. Alla, S. Polepalli, N. Jain, Synthesis and antiproliferative activity of imidazo [1, 2-a] pyrimidine Mannich bases, Eur. J. Med. Chem., 100 (2015) 18-23.

[23] X. Zhu, F. Wang, H. Li, W. Yang, Q. Chen, G. Yang, Design, synthesis, and bioevaluation of novel strobilurin derivatives, Chin. J. Chem . 30 (2012) 1999-2008.

[24] K. Kawai, K. Kaneko, N. Kaneko, Y. Shishino, K. Okamoto, Additive for imparting ultraviolet absorbency and/or high refractive index to matrix, and resin member using same, Miyoshi oil & fat Co. Ltd. Tokyo, Tokyo Optical Co. Ltd., Japan, 2017.

[25] K. Yofu, Curable resin composition, water-soluble ink composition, ink set, and image-forming method, Fuji Film Corporation, Tokyo, Japan, 2015.

[26] H. Matsushima, S. Hait, Q. Li, H. Zhou, M. Shirai, C.E. Hoyle, Non-extractable photoinitiators based on thiol-functionalized benzophenones and thioxanthones, Eur. Polym. J., 46 (2010) 1278-1287.

[27] J. Wei, F. Liu, Novel highly efficient macrophotoinitiator comprising benzophenone, coinitiator amine, and thio moieties for photopolymerization, Macromolecules, 42 (2009) 5486-5491.

[28] S. Jauk, R. Liska, Photoinitiators with functional groups, 8-benzophenone with covalently bound phenylglycine, Macromol. Rapid Commun., 26 (2005) 1687-1692.

[29] G. Odian, Principles of polymerization, John Wiley & Sons, 2004.

[30] W. Chen, X. Liu, l. Wang, J. Zhao, G. Zhao, Synthesis and preliminary photopolymerization envaluation of photopolymerizalbe type II photoinitiators BRA and TXRA, Prog. Org. Coat., 133 (2019) 191-197.

[31] X. Nan, Y. Huang, Q. Fan, J. Shao, High performance of the linked visible photoinitiator for free radical polymerization based on erythrosine B derivative, J. Appl. Polym. Sci., 132 (2015) 42361.

[32] C. Schmidt, T. Scherzer, Monitoring of the shrinkage during the photopolymerization of acrylates using hyphenated photorheometry/near‐infrared spectroscopy, J. Polym. Sci., Part B: Polym. Phys., 53 (2015) 729-739.

[33] K. Wang, S. Jiang, J. Liu, J. Nie, Q. Yu, Benzophenone-di-1, 3-dioxane as a novel initiator for free radical photopolymerization, Prog. Org. Coat., 72 (2011) 517-521.